nature portfolio

https://doi.org/10.1038/s41586-022-05281-0

Supplementary information

Fast charging of energy-dense lithium-ion batteries

In the format provided by the authors and unedited

Supplementary Information for

Fast Charging of Energy-Dense Lithium-Ion Batteries

Chao-Yang Wang, Teng Liu, Xiao-Guang Yang, Shanhai Ge, Nathaniel V. Stanley, Eric S. Rountree, Yongjun Leng and Brian D. McCarthy

Correspondence to: cxw31@psu.edu and bmccarthy@ecpowergroup.com

This PDF file includes:

Table S1. Design parameters for various electrodes used in this work

	Properties	**Energy-dense+**	**Energy-dense**	**Energy-dense high porosity**
Anode	Active material	artificial graphite		
	BET area	2.0 m^2/g		
	Mass Loading	13.4 mg/cm^2	10.8 mg/cm^2	
	Areal capacity	4.65 mAh/cm^2	3.75 mAh/cm^2	
	Porosity	0.26		0.35
	Cu foil thickness	8 μm		
Cathode	Active material	$LiNi_{0.8}Mn_{0.1}Co_{0.1}O_2$ (NMC811)		
	Mass Loading	21.3 mg/cm^2	17.2 mg/cm^2	
	Areal capacity	4.2 mAh/cm^2	3.4 mAh/cm^2	
	Porosity	0.30		
	Al foil thickness	13 μm		
Separator		Celgard-2325 microporous tri-layer membrane		
Weight		68 g	65 g	50 g
Capacity		4.5 Ah	4.2 Ah	3.2 Ah
Specific Energy	Test cell	243 Wh/kg	237 Wh/kg	228 Wh/kg
	50 Ah (estimated in pouch cell)	283 Wh/kg	271 Wh/kg	265 Wh/kg

Table S2. Design of the 150Ah prismatic cell with 4 nickel foils for 12S1P pack

Active materials	Anode	Graphite
	Cathode	NCM 811
Specific capacity of active material, Ah/g	Anode	0.350
	Cathode	0.193
N/P ratio		1.1
Loading of electrode (single-side), mg/ cm^2	Anode	10.8
	Cathode	17.2
Porosity, %	Anode	30
	Cathode	30
Active material: super P: CMC/SBR	Anode	97.7 : 0 : 1.0/1.3
Active material: super P: PVDF	Cathode	97.7 : 1.0 : 1.3
Current collector thickness, um	Cu foil	8
	Al foil	13
Electrode thickness, um	Anode	148.4
(double side coating include metal foil)	Cathode	120.5
Electrode size, cm	Anode	36.7×8.3
	Cathode	36.3×8.0
No. of electrodes	Anode	81
	Cathode	80
Separator thickness, um		25
Electrolyte, g		286
Number of nickel resistor sheets		4
Thickness of nickel resistor sheets, um		20
Thickness of insulation layer coated on resistor sheet, um		10
Location of nickel resistor sheets		10^{th}, 30^{th}, 50^{th}, 70^{th} of anode layers.
Cell size (length × height × thickness), cm		36.7× 8.65 × 2.8
Thickness of aluminum can, cm	Cap	0.15
	Bottom	0.05
	Others	0.025
Weight of aluminum can, g		219
Cell capacity, Ah		150.7
Weight of cell, g		2226.2
Specific energy, Wh/kg		**251**
Energy density, Wh/L		**627**

Fig. S1. Approaches to affordable battery energy. A) Gross cell weight vs. specific energy under different pack sizes. Starting from the state of the art (SoA) to two next-generation packs: 120 kWh pack with next-generation high energy batteries and 60 kWh pack with energy-dense batteries capable of fast charging. B) Time consumption vs. travel distance for EVs with different cruise ranges and charge time.

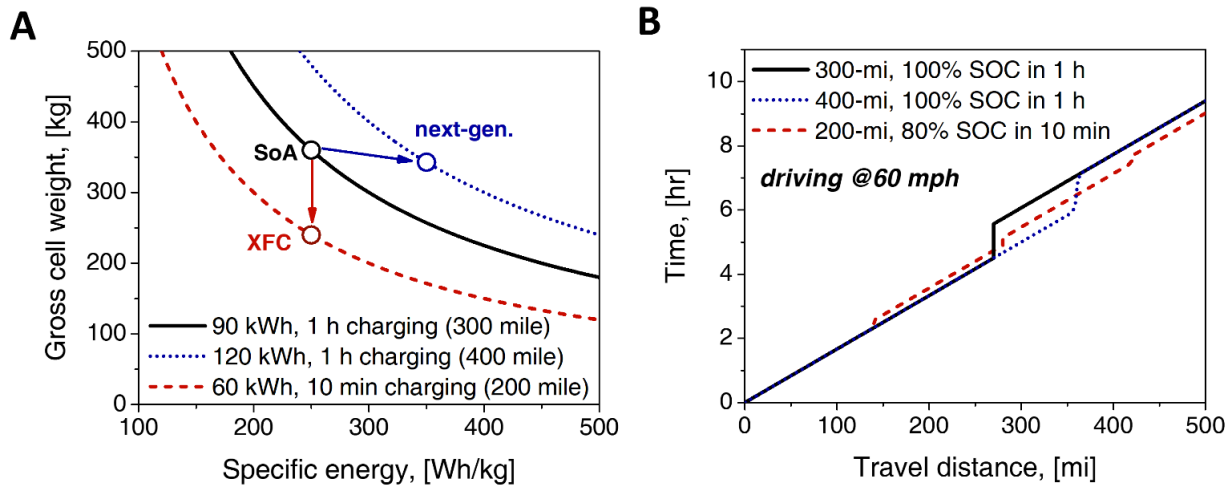

The equation to calculate curves for Fig. S1-A:

$$\text{gross cell weight} = \frac{\text{pack energy}}{\text{specific energy}}$$

For Fig. S1-B, we assume 10% capacity is retained before charging, and a 4-minute interstate ramp-XFC station-interstate time.

Fig. S2. Estimated energy density of various batteries in a 50-Ah format. The specific energies are assumed to be 85% of the theoretical values.

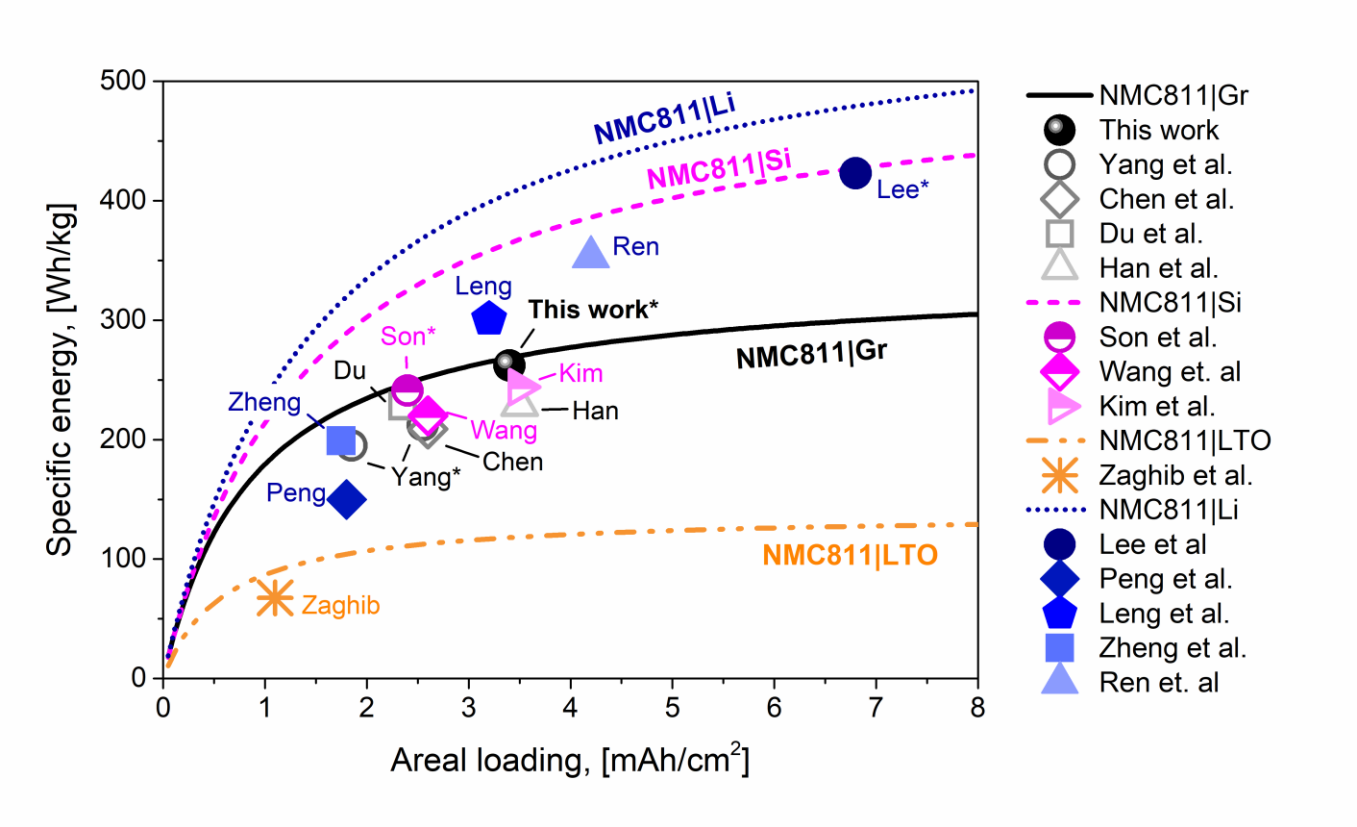

Fig. S3. Strategies to enhance ion transport in electrolyte. A) ionic conductivity and transference number of salts in EC-based electrolyte. B) influence of electrode porosity.

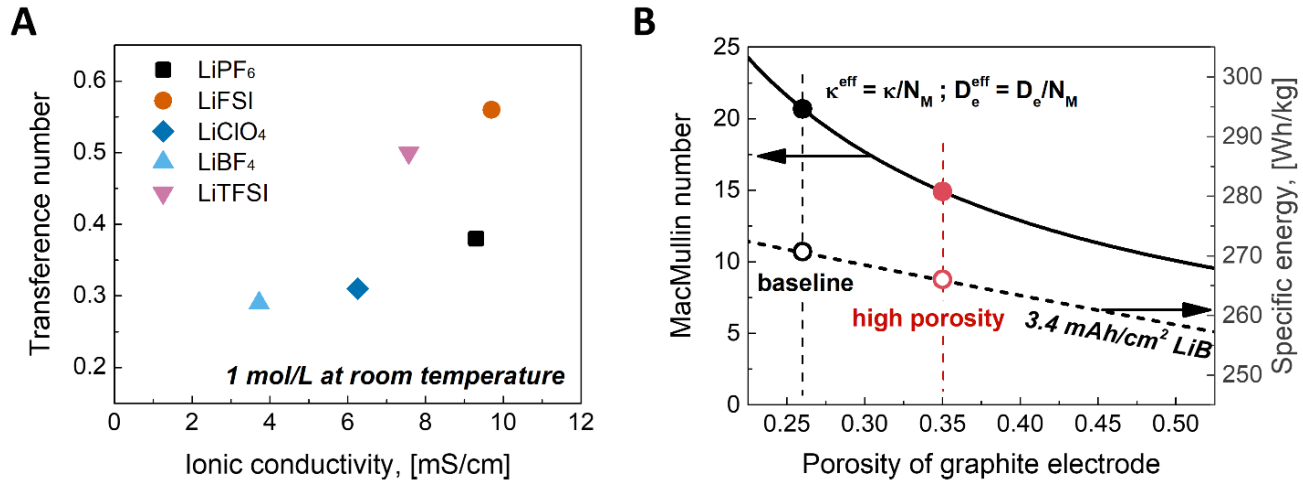

ECT Model

The ECT model used in this work describes the 1D electrochemical processes through the porous electrode, with Li diffusion in spherical particles accounted for by the so-called pseudo-2D approach.

- The reaction current (i) is related to the surface overpotential by the Butler-Volmer equation. Where the exchange current density (i_0) determines the kinetics of lithium insertion/deintercalation at the active material/electrolyte interface.

$$i = i_0 \left[\exp\left(\frac{\alpha_a F}{RT} \eta \right) - \exp\left(-\frac{\alpha_c F}{RT} \eta \right) \right] \quad \text{(S1)}$$

- The surface overpotential (η) is the potential difference between the solid and electrolyte phase at the reaction interface, driving electrochemical reaction. When $\eta > 0$, the reaction is dominated by the anodic reaction (lithium deintercalation); when $\eta < 0$, the reaction is dominated by the cathodic reaction (lithium insertion).

$$\eta = \Phi_s - \Phi_e - U - iR_f \quad \text{(S2)}$$

- Effective parameters in a porous medium are expressed as a function of porosity and Bruggeman exponents to account for tortuosity. Higher porosity results in higher effective transport values in the electrolyte but smaller effective values in the solid phase.

$$\Psi_s^{eff} = (1-\varepsilon)^p \Psi_s, \Psi_e^{eff} = \varepsilon^p \Psi_e \quad \text{(S3)}$$

- Volumetric current density (j) is the source term in charge conservation equations, which can be obtained by multiplying the specific surface area (a_s) with the electrode current density. The value of a_s is computed by assuming spherical particles.

$$j = a_s i, \; a_s = 3(1-\varepsilon)/r_i \quad \text{(S4)}$$

- Charge conservation in the solid phase describes the voltage drop caused by the ohmic resistance in electrodes. Usually, the potential drop in the solid phase is much smaller than that in the electrolyte phase, and thus is negligible.

$$\frac{dI_s}{dx} = \frac{d}{dx}\left(-\sigma^{eff} \frac{d\Phi_s}{dx} \right) = -j \quad \text{(S5)}$$

- Charge conservation in the electrolyte consists of two parts: the first part describes the voltage drop caused by the ohmic resistance in the electrolyte; the second part describes the concentration overpotential, which comes from the concentration gradient of the electrolyte.

$$\frac{dI_e}{dx} = \frac{d}{dx}\left(-\kappa^{eff} \frac{d\Phi_e}{dx} - \kappa_D^{eff} \frac{d\ln c_e}{dx} \right) = j,$$
$$\text{where } \kappa_D^{eff} = \frac{2RT\kappa^{eff}}{F}\left(t_+^0 - 1\right)\left(1 + \frac{d\ln f_{\pm}}{d\ln c_e}\right) \quad \text{(S6)}$$

- Species conservation in the electrolyte is governed by a diffusion process, with a non-zero migration term if the transference number (t_+) for Li-ion is less than one. The distribution of electrolyte concentration (c_e) is described by this equation, which determines the magnitude of concentration overpotential. The surface kinetics is also influenced by the value of c_e.

$$\frac{d}{dt}\left(\varepsilon c_e\right) = \frac{d}{dx}\left(D_e^{eff} \frac{dc_e}{dx} \right) + \left(\frac{1 - t_+^0}{F} \right) j \quad \text{(S7)}$$

- Species conservation in the active material particles is given by Fick's law. The value of lithium stoichiometry in solid particles is determined by this equation. The equilibrium potential of the active material is determined by the lithium stoichiometry on the particle surface.

$$\frac{\partial c_s}{\partial t} = \frac{1}{r^2}\frac{\partial}{\partial r}\left(r^2 D_s \frac{\partial c_s}{\partial r} \right), -D_s \frac{\partial c_s}{\partial r}\bigg|_{r=R_0} = \frac{i}{F} \quad \text{(S8)}$$

- Heat generation is calculated by the equation below. The heat generation comes from four components, namely: heat generation at the reaction interface (q_i), ohmic heat generation through the solid electrodes (q_s), heat generation through the electrolyte (q_e), and reversible heat (q_{rev}).

$$\begin{aligned} Q_{gen} &= A_E \int_0^L (q_i + q_s + q_e + q_{rev})\, dx \\ q_i &= j(\Phi_s - \Phi_e - U) \\ q_s &= I_s(-\frac{d\Phi_s}{dx}) = \sigma_s^{eff}(\frac{d\Phi_s}{dx})^2 \\ q_e &= I_e(-\frac{d\Phi_e}{dx}) = \kappa^{eff}(\frac{d\Phi_e}{dx})^2 + \kappa_D^{eff} \frac{d\ln c_e}{dx}\frac{d\Phi_e}{dx} \\ q_{rev} &= j(T\frac{dU}{dT}) \end{aligned} \quad \text{(S9)}$$

- The energy conservation equation determines the evolution of battery temperature in the form of a lumped model.

$$mc_p \frac{dT}{dt} = \dot{Q}_{gen} - h\left(T - T_\infty\right) A_s \quad \text{(S10)}$$

- The thermal dependence of electrochemical properties is described by the Arrhenius equation. With the battery temperature solved by the lumped thermal model, the electrochemical properties are updated according to:

$$\Psi\left(T\right) = \Psi_{ref} \exp\left(\frac{E_{act}}{R} \left(\frac{1}{T_{ref}} - \frac{1}{T}\right) \right) \quad \text{(S11)}$$

- The onset of lithium plating is determined by the lithium deposition potential. When $\eta_{Li|Li+} < 0$ V (or the surface overpotential of lithium insertion exceeds the equilibrium potential on graphite surface), Li-ions start to deposit on the graphite surface (*1*).

$$\eta_{Li|Li+} = U - |\eta_{LixC6|Li+}| \quad \text{(S12)}$$

The modeling parameters are listed in Table S3; the electrolyte properties and the equilibrium potential for graphite are provided in Fig.S4 and Fig.S5.

Table S3. Modeling parameters for active materials and separator

Properties	**Graphite (Li_xC_6)**	**Separator**	**$Li_xNi_{0.8}Mn_{0.1}Co_{0.1}O_2$**
Particle radius, r [μm]	10 A	-	3 B
Exchange current density, i_0 [mA/cm^2]	$0.21[2x^{0.5}c_e^{0.5}(1-x)^{0.5}]$ C (*49*, *50*)	-	$0.2[2x^{0.5}c_e^{0.5}(1-x)^{0.5}]$ B
Activation energy of i_0, $E_{act}^{i_0}$ [kJ/mol]	65 C (*51*, *52*)	-	65 B
Charge transfer coefficient, α_a, α_c	0.5, 0.5 A	-	0.5, 0.5 A
Solid state diffusivity, D_s [cm^2/s]	$2e\text{-}10\ (1.5\text{-}x)^{1.5}$ C (*53*)	-	$2e\text{-}10\ (1.5\text{-}x)^{1.5}$ B
Activation energy of D_s, $E_{act}^{D_s}$ [kJ/mol]	38 C (*54*)	-	21 B
Bruggeman factor, p	2.2 C (*36*)	2 C (*36*)	2.1 B
Specific heat of cell, c_p [J/(kg·K)]	1200 C (*55*)		
A, measured/calculated/commonly-used values. **B, fitted from simulation-experiment comparison.** **C, obtained from the literature.**			

Table S4. Thermal parameters for 3D pack simulations using GT-AutoLion3D

Parameter	Unit	Value
Thermal Conditions		
Ambient Temperature	°C	25
Heat Transfer Coefficient	(W/m2*K)	140
Thermal Properties of Electrode-Separator Layers		
Specific Heat Capacity	(J/kg*K)	1000
Thru-plane Thermal Conductivity	(W/m*K)	0.55
In-plane Thermal Conductivity	(W/m*K)	45.5
Thermal Properties of Metal Case		
Specific Heat Capacity	(J/kg*K)	1250
Thermal Conductivity	(W/m*K)	90

Fig. S4. Electrolyte properties. A) ionic conductivity, B) ionic diffusivity, and C) $dlnf_{\pm}/dlnc_e$ vs. electrolyte concentration.

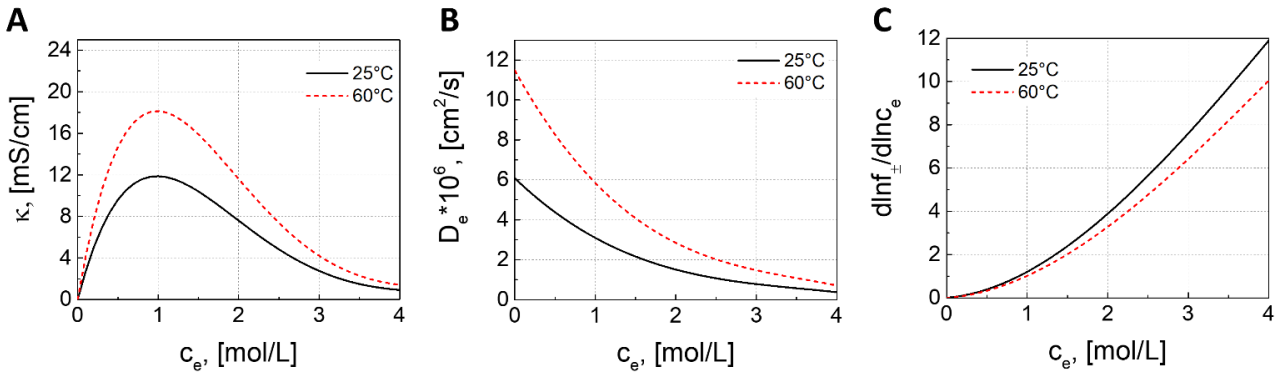

Fig. S5. Equilibrium potential of graphite vs. lithium stoichiometry.[52]

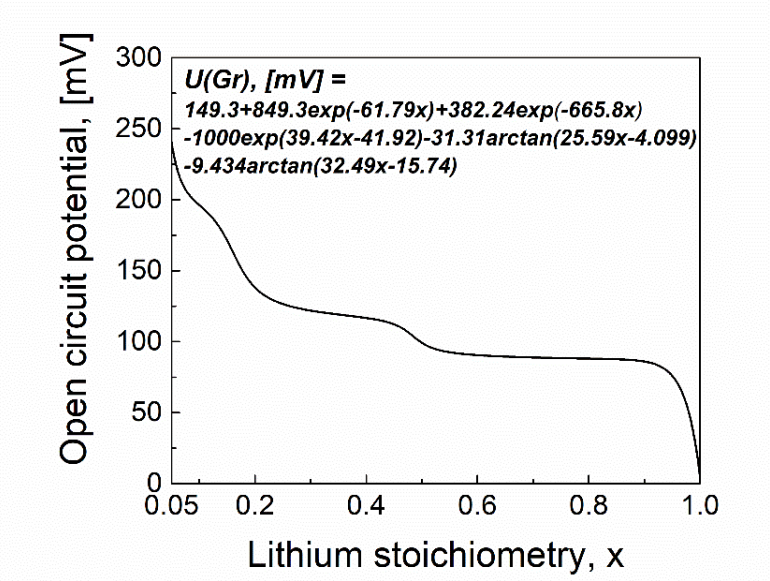

Equivalent Circuit for EIS

The first compoent is an inductance, which comes from the structure of pouch cells (for coin cells, this value is usually negalegible).

$$Z_L = i\omega L \tag{S13}$$

The second one is the high frequence resistance, representing the ohmic resistance of the battery.

$$Z_{HFR} = R_s + R_e + R_{cont} \tag{S14}$$

The third component consists of a resistor in parallel with a constant phase element (CPE); this component represents the impedance comes from the charge transfer process in the passive layers.

$$\begin{aligned} &Z_1 = R_{ct1} \cdot CPE_1 / (R_{ct1} + CPE_1), \\ &CPE_1 = 1/(\omega Q_1)^{\phi 1} \end{aligned} \tag{S15}$$

The fourth component describes the charge transfer process at the reaction surface of the active materials, the Warburg element is used to describe the diffusional impedance.

$$\begin{aligned} &Z_2 = (R_{ct2} + Z_W) CPE_2 / (R_{ct2} + Z_W + CPE_2), \\ &CPE_2 = 1/(\omega Q_2)^{\phi 2}, Z_W = A_W / \sqrt{i\omega} \end{aligned} \tag{S16}$$

Besides, a correction of transmission-line model is applied to this component to involve the ionic resistance in the electrolyte phase. The value of *l* equals to the thickness of porous electrodes.

$$Z_{2,TML} = \sqrt{Z_2 \cdot l / \kappa^{eff}} \coth(\sqrt{l/(Z_2 \cdot \kappa^{eff})}) \tag{S17}$$

The mathematical expresssion of the the total impedance equals to sum of the four compnents, and is fitted with the experimental results to get the magnitude of different components.

$$Z = Z_L + Z_{HFR} + Z_1 + Z_{2,TML} \tag{S18}$$

We chose the charge transfer resistance as one variable as it is directly related to graphite surface kinetics and determines whether Li ions undergo intercalation or graphite surface deposition. The ion transport resistance is chosen as the second matrix variable because it dominates the mass transport limitation in thick electrodes. Using the electrochemical properties of a baseline cell at 60°C as the reference, a property matrix was calculated to predict the lithium plating free (LPF) region as shown in the shaded areas. It is seen that the LPF region can be enlarged by increasing the electrolyte transference number or reducing the cutoff SOC during fast charging. Also, rational refinement of the cell design – such as adopting high porosity anodes to decrease the MacMullin number – can move a cell deeper into the LPF region (as shown by the empty symbol in Extended Data Fig.7b, where the relative ion transport resistance decreases to ~0.7). Alternatively, in a chemistry-agnostic approach elevating the charging temperature shifts the fast-charging battery into the LPF region. It is further shown that the limiting step of 4C charging energy-dense batteries lies in the ion-transport process, and that the LPF regions have a very narrow range in the axis of ion-transport resistance (Extended Data Fig.7b). Even if we elevate the charging temperature to 60°C, the ion transport property is still on the border of destructive lithium plating. Increase in the ion transport resistance during cycling may trigger lithium deposition for aged batteries and lead to the capacity rollover. Evolution of the experimental resistances during cycling is shown in Extended Data Fig.7c,d. Both charge transfer resistance and ion transport resistance for the baseline cell ($t_+ = 0.38$ and $\varepsilon = 0.26$, respectively) increases much faster than the cells with enhanced ion transport ($t_+ = 0.48$, $\varepsilon = 0.35$), confirming the effectiveness of combined use of dual-salt electrolyte and high-porosity anode.

NEW REFERENCES NOT CITED IN MAIN TEXT

49. P. Arora, Mathematical Modeling of the Lithium Deposition Overcharge Reaction in Lithium-Ion Batteries Using Carbon-Based Negative Electrodes. *J. Electrochem. Soc.* **146**, 3543 (1999).

50. X. Yang, C. Wang, Understanding the trilemma of fast charging , energy density and cycle life of lithium-ion batteries. *J. Power Sources*. **402**, 489–498 (2018).

51. R. V. Bugga, M. C. Smart, (2010; http://ecst.ecsdl.org/cgi/doi/10.1149/1.3393860), vol. 25, pp. 241–252.

52. Y. Ji, Y. Zhang, C.Y. Wang, Li-Ion Cell Operation at Low Temperatures. *J. Electrochem. Soc.* **160**, A636–A649 (2013).

53. M. D. Levi, D. Aurbach, Diffusion Coefficients of Lithium Ions during Intercalation into Graphite Derived from the Simultaneous Measurements and Modeling of Electrochemical Impedance and Potentiostatic Intermittent Titration Characteristics of Thin Graphite Electrodes. *J. Phys. Chem. B*. **101**, 4641–4647 (1997).

54. N. Takami, Structural and Kinetic Characterization of Lithium Intercalation into Carbon Anodes for Secondary Lithium Batteries. *J. Electrochem. Soc.* **142**, 371 (1995).

55. L. Sheng, L. Su, H. Zhang, Y. Fang, H. Xu, W. Ye, An improved calorimetric method for characterizations of the specific heat and the heat generation rate in a prismatic lithium ion battery cell. *Energy Convers. Manag.* **180**, 724–732 (2019).